THE JOURNAL OF PHYSICAL CHEMISTRY B

Article

pubs.acs.org/JPCB

Compact and Blinking-Suppressed Quantum Dots for Single-Particle Tracking in Live Cells

Lucas A. Lane,[†] Andrew M. Smith,[‡] Tianquan Lian,[§] and Shuming Nie*[,†]

[†]Departments of Biomedical Engineering and Chemistry, Emory University and Georgia Institute of Technology, Atlanta, Georgia 30322, United States

[‡]Department of Bioengineering, University of Illinois at Urbana−Champaign, Urbana, Illinois 61801, United States

[§]Department of Chemistry, Emory University, Atlanta, Georgia 30322, United States

Supporting Information

ABSTRACT: Quantum dots (QDs) offer distinct advantages over organic dyes and fluorescent proteins for biological imaging applications because of their brightness, photostability, and tunability. However, a major limitation is that single QDs emit fluorescent light in an intermittent on-and-off fashion called "blinking". Here we report the development of blinking-suppressed, relatively compact QDs that are able to maintain their favorable optical properties in aqueous solution. Specifically, we show that a linearly graded alloy shell can be grown on a small CdSe core via a precisely controlled layer-by-layer process, and that this graded shell leads to a dramatic suppression of QD blinking in both organic solvents and water. A substantial portion (>25%) of the resulting QDs does not blink (more than 99% of the time in the bright or "on" state). Theoretical modeling studies indicate that this type of linearly graded shell not only can minimize charge carrier access to surface traps but also can reduce lattice defects, both of which are believed to be responsible for carrier trapping and QD blinking. Further, we have evaluated the biological utility of blinking-suppressed QDs coated with polyethylene glycol (PEG)-based ligands and multidentate ligands. The results demonstrate that their optical properties are largely independent of surface coatings and solvating media, and that the blinking-suppressed QDs can provide continuous trajectories in live-cell receptor tracking studies.

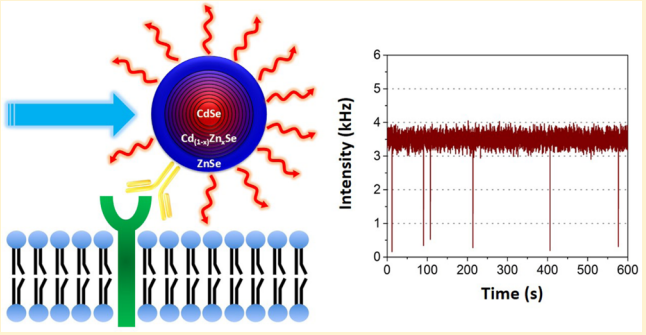

INTRODUCTION

Quantum dots (QDs) are photoluminescent nanocrystals composed of semiconductor materials that are the subject of multidisciplinary interests across the biomedical, electrical, and physical sciences.[1−5] For biological imaging applications, QDs offer several distinct advantages over fluorescent organic molecules and proteins.[6−10] For example, QDs can emit light over a broad range of wavelengths covering the entire visible and near-infrared regions of the electromagnetic spectrum by tuning both particle size and chemical composition.[11−14] Also the emission from QDs can be considerably brighter than that of traditional fluorophores owing to greater absorption cross sections, leading to improved signal-to-noise ratios in fluorescence imaging experiments. A high signal-to-noise ratio is especially important for single molecule imaging and tracking experiments in order to obtain nanometer precision of the probe location.[15]

Single molecule tracking has been performed using probes that either scatter or emit light,[5−7] but there are significant trade-offs associated with all the probes employed to date.[16] Organic dyes and proteins have small sizes, which minimally perturb the native dynamics of the molecule being tagged. However, these probes suffer from rapid photobleaching, limiting observation to only a few seconds before irreversible photobleaching.[17] Light scattering from metal particles is exceptionally stable, but the large particle sizes needed for observation increase their drag forces, leading to reduced diffusion rates. As a balance between these extremes, QDs have greater photostability than organic dyes and proteins, allowing long-duration observation while being smaller than gold particles, which lessens perturbations to the natural diffusion of the tagged molecules.

However, a major limitation in using QDs for single-particle tracking is that single QDs emit fluorescent light in an intermittent on-and-off fashion called "blinking."[9] The non-fluorescent or "off" periods of currently available QDs can have durations up to 100 s, which leads to frames without probe signals (see Figure 1). Algorithms have been developed to reconstruct the missing positions,[18−22] but they have limited accuracy for long off states, especially when the observed field

Special Issue: Spectroscopy of Nano- and Biomaterials Symposium

Received: June 28, 2014
Revised: August 25, 2014
Published: August 26, 2014

   dx.doi.org/10.1021/jp5064325 | J. Phys. Chem. B 2014, 118, 14140−14147

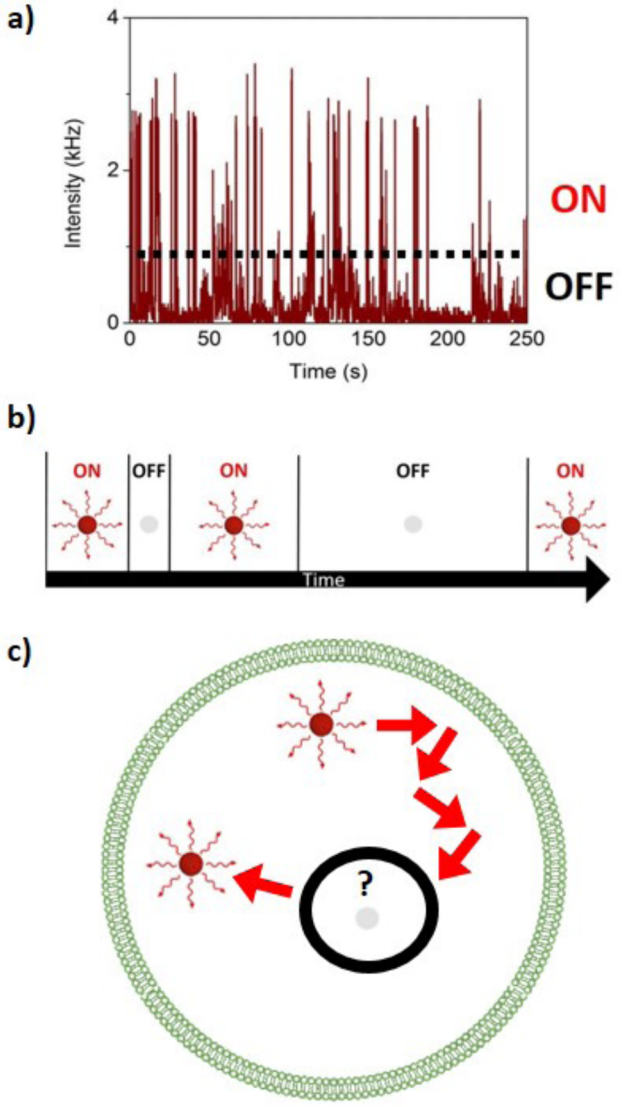

Figure 1. (a) Intermittent fluorescence emission (blinking) observed in a dynamic intensity trace of a conventional core/shell QD (CdSe/ZnS). The dotted line on the dynamic trace indicates the demarcation between on and off states. Note that occasional "grey states" can appear, which are at intensity values above the background but below the average intensity of the on states. (b) Depiction of random switching between fluorescent (on) and nonfluorescent (off) states under continuous laser excitation. (c) Illustration of an uncertainty region in the trajectory of a QD upon entering a prolonged off state in a single-particle tracking experiment.

contains multiple mobile QDs and the environment is physically heterogeneous, such as the membrane of a cell.[23] Thus, there is a great need to suppress this blinking behavior in order to realize the benefits of photostable QDs for use in single-molecule imaging.

Suppression of QD blinking was first reported by Ha and co-workers, who passivated the QD surface by using small thiolate reagents such as mecaptoethnaol.[24] It is believed that small thiolate molecules are packed densely on the QD surface to satisfy the many unpassivated cations that often act as electron traps. Having small thiolated molecules donating electrons to surface trap states reduces the number of traps accessible to electrons ejected from the QD core, thus suppressing the charge-trapping pathway of blinking. Another approach in preventing carrier access to surface traps is to grow a thick shell of a higher band gap material around the QD core, otherwise known as a "giant" shell structure, to limit carrier tunneling to the particle surface. Such structures have been synthesized using the CdSe/CdS core/shell system and have been observed to suppress blinking.[25,26]

Suppression of blinking has also been reported by tailoring the electronic band potential profile of core−shell QDs. The main rationale is that in conventional core/shell QDs, which have an abrupt transition between the core and shell materials, charge carriers can obtain ample momentum from the uncertainty at potential profile discontinuities to contribute to an Auger excitation process.[27] On the other hand, QDs with a smooth potential that is free of discontinuities could lower Auger rates several orders of magnitude relative to traditional core/shell particles by relaxing the momentum uncertainties.[27] An experimental study supporting this theory was performed through creating a smooth confinement potential resembling a parabola originating from $Cd_{1-x}Zn_xSe$/ZnSe alloy-core/shell particles, where x gradually changes from 0 at the center to 1 at the surface of the QD.[28] The authors demonstrated a complete absence of blinking for up to hours of continuous excitation. However, the general applicability of this mechanism is still a matter of debate because the earlier results have not been reproduced or confirmed.

Despite these advances in blinking suppression, there are still major limitations in using QDs for biological imaging and tracking studies. Blinking suppression using small thiolated compounds requires reagent concentrations in the millimolar range, which is highly toxic to cells.[29] Giant QDs, with sizes near 20 nm,[25] are about twice the hydrodynamic size of IgG,[30] which can significantly alter the dynamics of the tagged biomolecule, especially when considering the additional size from the solvating ligands required to stabilize the particle in solution. Though there have been reports showing blinking suppression using fewer monolayers of CdS shell surrounding a CdSe core than the giant QDs,[31,32] it has yet to be demonstrated that these particles maintain blinking suppression after transfer to aqueous solution.

In this work, we report a new strategy to synthesize blinking-suppressed QDs based on a generalizable gradient alloy structure and robust synthesis approach similar to that employed for giant shell QDs. Specifically, we show that a linearly graded shell can be prepared in a stepwise, automated fashion, leading to a new class of QDs with precisely controlled chemical compositions and potential profiles. By spreading the lattice strain between two mismatched materials across a large number of atoms, we have used this graded alloy approach not only to minimize internal and interfacial lattice defects (to avoid carrier trapping), but also to minimize carrier propagation probabilities at the particle surface (also to avoid carrier trapping). It should be noted that analogous methods are routinely applied in the electronics industry to avoid interfacial defect formation by linearly grading a substrate (e.g., silicon) to a lattice-mismatched epitaxial layer (e.g., germanium). Our results show that this method produces relatively compact, blinking-suppressed QDs with favorable optical properties that are independent of surface ligands or solvating media. These probes are well-suited for live-cell single-particle tracking studies where they exhibit continuous trajectories.

dx.doi.org/10.1021/jp5064325 | J. Phys. Chem. B 2014, 118, 14140−14147

METHODS

Chemicals. All chemicals were purchased from Sigma-Aldrich and used without further purification or modification unless otherwise stated: 1-ocadecene (ODE, 90%), 1-tetradecene (TDA, 92%), selenium powder (Se, 99.99%), octadecylamine (ODA, 90%), trioctylphosphine (TOP, 97%), cadmium oxide (CdO, 99.99%), dioctylamine (DOA, 98%), diethylzinc (1.0 M in hexanes), oleylamine, thioctic acid (TA, 98%), 4-(*N*,*N*-dimethylamino)pyridine (DMAP, 99%), *N*,*N*-dicyclohexylcarbodiimide (DCC, 99%), sodium borohydride (NaBH4, 99.99%), poly(acrylic acid) (PAA, MW 1773), *N*-hydroxysuccinimide (NHS, 98%), *N*,*N*′-diisopropylcarbodiimide (DIC, 98%), cysteamine (95%), 1-thioglycerol (97%), dimethyl sulfoxide (DMSO, 99.9%), dimethylformamide (DMF, 99.8%), methoxypolyethylene glycol amine (750 MW), and poly(ethylene glycol) methyl ether thiol (5000 MW). Dimethylcadmium (10 wt % in heptane) and bis-(trimethylsilyl)selenide ($(TMS)_2Se$) were obtained from Gelest. Tetradecylphosphonic acid (TDPA, 99%) was purchased from PCI Synthesis. *N*-Fmoc-ethylenediamine (Fmoc-EDA) was purchased from ABD Bioquest.

Synthesis of CdSe Cores. Approximately 0.6 mmol of CdO and 1.4 mmol of TDPA were added to a 250 mL flask with 25 mL of ODE. The mixture was heated to 120 °C under vacuum for 2 h to remove water and oxygen. After purging 3 times with argon, the mixture was heated to 320 °C under inert gas until the solution became clear. The mixture was then cooled to room temperature and 6 g of ODA was added. Again, the solution was heated to 120 °C for 2 h under vacuum and then purged three times with argon. In a separate 100 mL flask, a 7.5 mL solution containing 0.4 M of TOP-Se in TOP was added. Here Se powder was added to TOP, where the flask was then evacuated and put in inert atmosphere in the same manner as the other reaction flask. Once under argon, the flask temperature was raised to 160 °C, where it was left overnight and then cooled to room temperature. The temperature in the cadmium precursor flask is set to 290 °C when the solution of TOP-Se is swiftly injected. After injection, the flask is immediately removed from the heating mantle and placed under forced air to quickly bring the solution to room temperature. Cores were then diluted to a 1:5 ratio of reaction solution in hexanes and centrifuged at 5000 rpm to remove insoluble cadmium precursors. The particles were then precipitated with acetone and washed several times in methanol and hexane extractions.

Synthesis of Linearly Graded Alloy Shells. Two-hundred nanomoles of the purified solution of CdSe cores was placed in a mixture of 5 mL of ODE and 5 mL of DOA. The solution was then heated to 110 °C under vacuum for 1 h and later purged with argon three times to remove water and oxygen. Shell addition for the graded alloy QDs was performed by introducing calculated amounts of glovebox-prepared 0.1 M solutions of dimethylcadmium and diethylzinc combinations in oleylamine and $(TMS)_2Se$ in TDE separately by a syringe pump at a rate of 0.5 mL/h. A single monolayer was deposited in a day then left to anneal overnight at 60−80 °C. Since the graded alloy proceeds in increments of $x = 0.1$ for each monolayer, and then an additional 4 monolayers of ZnSe are added, the total reaction time is 14 days. Shell growth temperatures start at 130 °C and work up to 240 °C as sequential layers are added to improve the crystallinity of the final products.

Ligand Synthesis and Phase Transfer Procedures. Thioctic acid conjugated to 750 molecular weight methoxypolyethylene glycol amine (TA-750PEG-OCH3) followed a similar procedure to that presented by Mei et al.,[33] where equimolar amounts of each are reacted with DMAP and DCC in methylene chloride. The disulfide bond was then reduced using $NaBH_4$ in a methanol and water solution. Preparation of the multidentate polymer followed the procedure outlined by Smith and Nie.[34] Here polyacrylic acid was functionalized with thiols and amines by adding cysteamine and Fmoc-ethyldiamine through DIC and NHS in DMSO, later deprotecting the amines by piperidine. Poly(ethylene glycol) methyl ether thiol of molecular weight 5000 Da (HS-5000PEG-OCH_3) is used without any modifications. For ligand transfer of the TA-750PEG-OCH3 and HS-5000PEG-OCH_3, QDs were performed similar to the method of Kang et al.,[35] where the QD solution and ligands are dissolved in chloroform, stirred under mild heating, and then PBS was introduced into the solution. Typical QD concentrations were ∼5 μM, and polymer concentrations were in slight excess of a 1 molar ratio of cations. The transfer method for the multidentate polymer follows the original procedure,[34] whereby QDs were first transferred to DMSO with thioglycerol ligands and polymer was introduced to the solution followed by heating to 80 °C for 2 h. All QDs were then purified by either 30 kDa centrifugal filters (Amicon) or 25 kDa dialysis tubing (Spectra/Por).

Characterization. Single QD fluorescence measurements were performed with a home-built system. The excitation source was a mode locked Ti:sapphire laser (Tsunami oscillator pumped by 10 W Millenia Pro, Spectra-Physics) operated at a wavelength of 800−1000 nm pulsed ∼100 fs at a 82 MHz repetition rate. The output is then sent through a pulse picker (Conoptics) to reduce the repetition rate by a factor of 9. In order to achieve shorter wavelengths needed for QD absorption, the light was passed through a frequency doubling β-BaB_2O_4 (BBO) crystal to achieve wavelengths of 400−500 nm. The sample dispersed on a microscope slide was placed on a piezo scanning stage (Mad City Laboratories), where laser illumination was focused to a diffraction-limited spot on the slide through the microscope objective (NA 1.4/100x oil, Olympus). A confocal ray path was created from a pinhole in the image plane where only the signal from the focal plane is transmitted. The signal from the focal plane was then collected through the same objective and focused to an avalanche photodiode (APD, Pelkin-Elmer, SPCM-AQR-14) with photon counting accomplished by a time-correlated single photon counting module (TCSPC, Becker&Hickel SPC 600). Single QDs on the slide were located through point-by-point scanning of the laser beam across the sample by the piezo scanner. In addition, single QDs were verified using an atomic force microscope (AFM, Asylum's MFP-3D-BIO)

Absorption spectra were obtained using a Shimadzu UV-2401PC scanning spectrophotometer. Photoluminescence spectra were acquired using a spectrofluorometer from Photon Technology International. Quantum yields were obtained by using a standard of fluorometric grade Rhodamine 6G (R6G) dye dissolved in methanol.

High-resolution TEM (HRTEM) of the resulting graded alloy shell QDs was performed using a Hitachi H-9500 operated at 300 kV. The mean particle size was determined by inspecting 200 different particles through the use of the analysis software ImageJ.

dx.doi.org/10.1021/jp5064325 | J. Phys. Chem. B 2014, 118, 14140−14147

The chemical composition of graded alloy QDs was determined through X-ray photoelectron spectroscopy (XPS) using a Thermo Scientific K-Alpha having an Al Kα source operated at 160 at 0.1 eV step size with 200 ms dwell time.

QD Biofunctionalization. First, sulfo-LC-SPDP was reacted with QDs having solvating ligands of DHLA-PEG3400-NH_2 (Nanocs) at room temperature for 1 h at a ratio of 10000 linkers per QD. Once the reaction is complete, the disulfide bond of the linker is reduced through adding an excess of DTT. The resulting QDs, presenting thiol end groups, were then purified with a desalting column equilibrated with PBS to remove unreacted sulfo-LC-SPDP along with DTT. In a separate vial, to introduce thiol reactive groups of maleimido to the antibody, the amine groups of anti-EGFR (Invitrogen 31G7) were activated by reacting with sulfo-SMCC at a ratio of 10 linking agents to 1 antibody. Excess SMCC linker was removed by membrane filtration (MWCO 30 kDa). Finally, the maleimido functionalized anti-EGFR was reacted with the surface thiol groups of the QDs in a 1.2:1 molar ratio for 3 h in PBS under vigorous mixing. The resulting QD-Ab conjugates were purified through size-exclusion column chromatography equilibrated with PBS.

Live Cell Single Particle Tracking. The human lung carcinoma cell line A549, which overexpresses EGFR, was grown on coverslips in a medium containing 10 mM HBSS, 10 mM HEPES, and 5% FBS, pH 7.4. For labeling, cells were first washed with PBS, then incubated at 4 °C for 30 min in 1% BSA in PBS and for 1 h with the QD-Ab conjugates in picomolar quantities. Unbound QDs were removed through washings of PBS. Imaging was performed with a wide field fluorescent microscope (Olympus IX 70) using a 100 W mercury lamp excitation source (Osram HBO 103w/1) with 560 ± 40 nm and 610 excitation and long pass filters, respectively. A region of interest was selected based on the bright field image of the cell. Once this region was chosen, the fluorescence image was then taken to observe the QDs present in the area. Once a well isolated QD had been spotted, real time fluorescence image recording was performed at 33 frames per second with a CCD camera (Hamamatsu C9100). The total duration of an imaging experiment did not exceed 15 min to ensure cell viability when tracking the surface receptors.

RESULTS AND DISCUSSION

Linearly Graded QDs. We synthesized core/shell/shell CdSe/$Cd_{1-x}Zn_xSe$/ZnSe QDs, for which the $Cd_{1-x}Zn_xSe$ region is linearly graded in composition from the core CdSe material to the outer shell ZnSe material, with x increasing in increments of 0.1 with each monolayer (see Figure 2a). The composition and structure of the multishell domains were chosen to simultaneously minimize interfacial lattice strain and to confine the charge carriers in a deep potential well. To insulate the charge carriers, it is necessary to use a shell material with larger bandgap than the core CdSe material (E_g = 1.76 eV). Because it is well-known that very large shells of CdS (E_g = 2.50 eV) are needed to adequately reduce blinking, we chose the wider bandgap ZnSe material (E_g = 2.82 eV), which has a larger conduction band offset from the core CdSe material to more strongly insulate the more mobile electron to prevent tunneling to the surface with a thinner shell. However, due to a general trend of decreasing bond length with increasing bandgap, greater insulation also increases the lattice mismatch with the core material, leading to a compressive strain in the core and a net tensile strain in the shell. Beyond a critical shell

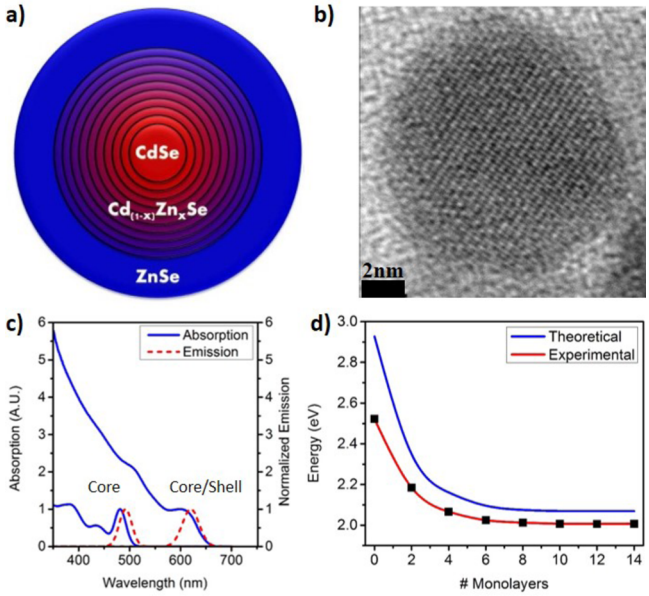

Figure 2. (a) Multilayer structure of the linearly graded shell material increasing in zinc content surrounding the core. (b) HRTEM images of a single CdSe/$Cd_{1-x}Zn_xSe$ linear step graded alloy shell QD. (c) Normalized absorption and emission spectra of the initial cores and the final core/shell particles. (d) Dependence of the exciton energy on shell thickness for CdSe/$Cd_{1-x}Zn_xSe$ core/shell particles. The red line depicts experimental emission values, and the blue line shows calculated values using the effective mass approximation for a core radius of 1.0 nm and a shell graded in linear steps of x = 0.1 with an additional 4 monolayers of pure ZnSe.

thickness, the strain energy will become large enough to cause the formation of lattice defects such as loop dislocations that act as carrier traps and Auger recombination sites, leading to reduced radiative excitonic recombination.[36] To offset the accumulation of strain at the core/shell interface, compositional grading was used to generate coherent epitaxial layers of the shell, as earlier work in semiconductor heteroepitaxy has demonstrated that graded alloys relieve interfacial strain and can prevent dislocation formation at the epitaxial−substrate interface where they are most likely to nucleate.[37,38]

Core CdSe nanocrystals with a diameter of 2.0 nm were synthesized using a hot-injection method and dispersed in a mixture of dioctylamine and octadecene for shell deposition. We used highly reactive shell precursors, diethylzinc, dimethylcadmium, and $(TMS)_2Se$, to enable efficient shell growth at low temperatures that are needed to prevent Ostwald ripening of the small cores, to balance cation activity, and to promote isotropic growth. Commonly used metal-oleates and TOP-Se typically require temperatures higher than the temperature at which CdSe ripens, and the reactivities of zinc-oleate and cadmium-oleate are drastically different.

The major ligand during shell growth is initially the secondary amine DOA, a softer Lewis base than primary amines. DOA balances the reactivity between zinc and cadmium precursors at the initial stages of shell growth, as zinc has a higher affinity toward primary amines and only weakly binds to the QD surface atoms to allow efficient shell growth at low temperatures. As subsequent shells are deposited with increasing zinc content, more primary amine is introduced into the system, since the cation precursors are dissolved in oleylamine, which becomes the major ligand on the nanocrystal

dx.doi.org/10.1021/jp5064325 | J. Phys. Chem. B 2014, 118, 14140−14147

surface. Primary amines are favored in the later stages of shell growth as they provide enhanced binding strength to the nanocrystal surface, affording greater colloidal stability beneficial for dispersion of larger particles with lower surface energy.

Shell precursors were added to the reaction vessel via syringe pump, and reaction progress was monitored by UV−vis, emission spectrophotometry, and transmission electron microscopy. After 14 monolayers of growth, chemical composition was determined through X-ray photoelectron spectroscopy (see Figure S1 of the Supporting Information). The final graded alloy QDs were highly crystalline, nearly spherical with a size of 10.1 ± 1.2 nm (see Figure 2**b**), and monodisperse (see Figure S2 of the Supporting Information). The fluorescent emission peak center is near 620 nm with a fwhm of 40 nm and has a quantum yield near 50%. Figure 2**c** shows that there is decreasing emission energy as more monolayers of shell material were added, while there is an increase in the absorption at shorter wavelengths. This is an indication of the charge carrier wave functions increasing in volume (less confined), along with an increase in the absorption cross section due to larger particle size (more oscillators). The energy profile with monolayer additions is qualitatively similar to that of what would be expected from theoretical calculations based on the effective mass approximation (see Figure 2d).

Single-Particle Studies. Samples of the CdSe cores and CdSe/$Cd_{1-x}Zn_xSe$/ZnSe QDs were compared at the single-particle level. Particles solvated in hexane solution were spun onto glass microscope slides and were observed under ambient conditions. Single QDs on the slide were located through point-by-point scanning of a focused laser beam and were further verified with atomic force microscopy (see Figure S3 of the Supporting Information). As shown in Figure 3 (panels a and b), there is a drastic change in total time spent between emissive and nonemissive states between the two samples. The cores without a shell are mostly in the off state during illumination, with few brief on states, whereas after shell growth the particles spend most of the time in the on state with few short off states. The probabilities of the on and off periods for the cores with and without the linearly graded alloy shells were fit to a power law distribution of the form $P \propto t^{-m}$, as shown in Figure 3 (panels c and d).[39] The power parameter for the "on" time, m_{on}, of the core alone was 1.83, while the "off" parameter, m_{off}, was 1.52. For the core/shell, the on and off probability parameters were m_{on} = 0.87 and m_{off} = 1.97, showing an increased probability of on events and decreased probability of off events. Similar changes encountered in power law parameters from the on and off distributions for traditional core and core/shell particles[40] have been observed when blinking suppression is achieved.[32,41] Of 100 particles inspected for the graded alloyed shell QDs, a large fraction of the population exhibited substantial blinking suppression, where almost a quarter of the population exhibited >99% on times with an ensemble average of 92.6 ± 8.1%, as shown in Figure 3e). In addition, the infrequent off times were of short durations, typically less than 200 ms (see Figure 3f).

The fluorescent lifetime of the graded shell QDs exhibited mostly monoexponential behavior (89% 24.3 ns, 11% 2.1 ns) having a characteristic lifetime of 24.0 ns (see Figure S4 of the Supporting Information). Such monoexponential lifetimes of the QD sample can be indicative of a high fraction of the probes being primarily in on states during excitation. Fisher et al. observed that both single and extrapolated ensemble

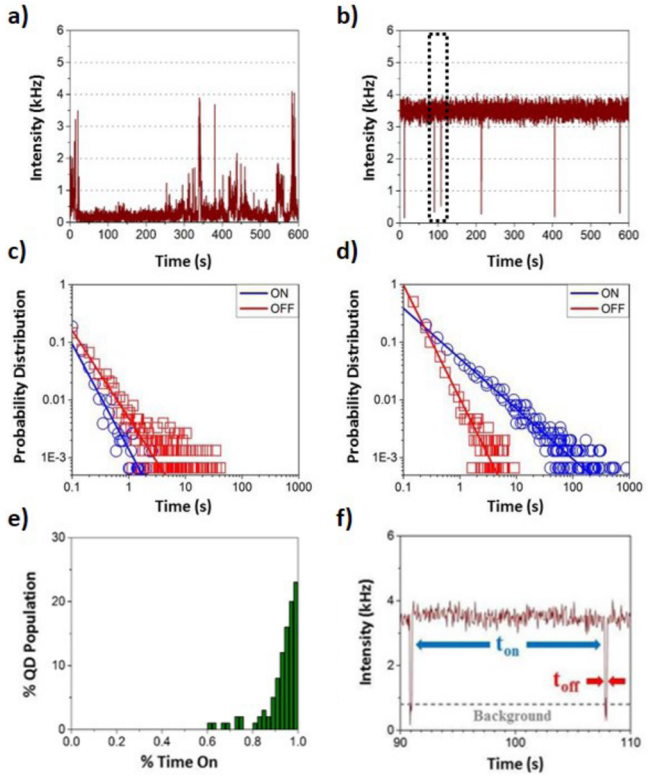

Figure 3. Dynamic fluorescence traces of (a) a 2.0 nm CdSe core and (b) the graded alloy core/shell QD along with the on/off time probability distributions for (c) the cores and (d) graded shell particles. (e) Histogram of the percentage of "on" times for an ensemble of 100 gradient alloy shell particles. (f) Expanded view of the intensity trace of the gradient alloy shell QD showing the short timescale "off" events and long-duration "on" events.

lifetimes of CdSe/ZnS QDs exhibit monoexponential behavior of fluorescence lifetimes if the fluorescence lifetime is only mapped for times where the single QD fluorescence exceeds the on state threshold.[42] As dark and gray states are introduced into the lifetime measurements, multiexponential behavior is observed due to nonuniform fluctuations in the nonradiative rates present between the individual particles.[42]

Bioconjugation. For application of QDs in biological experiments, the particles synthesized in organic solvents must be transferred to an aqueous phase. Three different ligands were chosen to replace the as-synthesized organic ligands: a single thiol-anchored PEG of 5000 molecular weight (HS-5000PEG-OCH3), a bidentate thiol-anchored PEG of 750 molecular weight (TA-750PEG-OCH3), and a thin-layer multidentate polymer with a mixture of thiol- and amine-anchoring groups (for their chemical structures, see Figure S5 of the Supporting Information).[34] After ligand exchange of the QDs, all particles were dispersed homogeneously in water. From DLS measurements, hydrodynamic diameters were 22 ± 4.1 nm, 19 ± 3.2 nm, and 14 ± 2.0 nm for HS-5000PEG-OCH3, TA-750PEG-OCH3, and the multidentate polymer, respectively.

Surprisingly, no significant change in quantum yield (<3%) was detected for any of the QDs after ligand exchange (Figure S6 of the Supporting Information). Decreases in quantum yield are typically observed upon ligand exchange in the aqueous solubilization of QDs; however, fluorescence efficiencies can be maintained if the shell potential barrier is sufficient to keep

dx.doi.org/10.1021/jp5064325 | J. Phys. Chem. B 2014, 118, 14140−14147

exciton carriers insulated within the core. Giant shell CdSe/CdS QDs were similarly observed to have quantum yields that were independent of the ligands present on the surface of the nanocrystal.[25]

The QDs coated with three different hydrophilic ligands were also compared in blinking behavior. Remarkably, the blinking suppression was invariant to the ligands in both the frequency and duration of the off times (see Figure 4). The

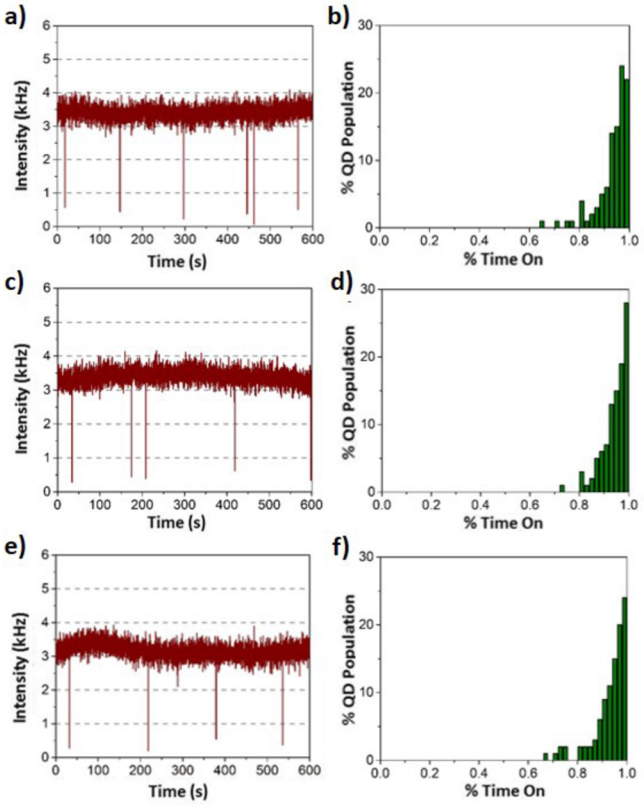

Figure 4. Dynamic intensity traces of the blinking-suppressed gradient alloy shell QDs with aqueous solvating ligands of (a) the minimized multidentate polymer, (c) TA-750PEG-OCH_3, and (e) SH-5000PEG-OCH_3, along with their corresponding on time percentage histograms of 100 particles inspected for 600 s each (b, d, f, respectively).

distributions of ensemble on time percentages were similar for QDs cast from hexane solution (92.6 ± 8.1%) and the QDs cast from aqueous solutions having coatings of multidentate polymers (93.1 ± 6.9%), TA-750PEG-OCH3 (94.2 ± 5.1%), and HS-5000PEG-OCH3 (93.5 ± 6.4%). To our knowledge, this is the first QD synthesis method that is able to preserve the optical properties of quantum yield and blinking suppression after aqueous transfer using a variety of ligands.

Receptor Tracking. To demonstrate the benefit of using blinking suppressed probes in live-cell single-molecule tracking, conventional core/shell QDs composed of CdSe/CdS/ZnS[43] with abrupt shell interfaces (AS-QDs) were compared to the blinking-suppressed CdSe/$Cd_{1-x}Zn_xSe$/ZnSe particles with gradient shells (GS-QDs). Both QDs were conjugated to an antibody against the epidermal growth factor receptor (EGFR) to track the receptors on live A549 cells and imaged using conventional wide-field epifluorescence microscopy. Both QDs had similar emission wavelengths of 630 and 620 nm, respectively; however, notable differences between the two probes were that the gradient QD conjugates were 5.0 nm larger in hydrodynamic diameter ($HD_{AS\text{-}QD}$ = 26 ± 5.8 nm and $HD_{GS\text{-}QD}$ = 31 ± 6.4 nm) and had slightly lower quantum yield of (50% compared to 65% for the AS-QDs). The AS-QDs had noticeable blinking, whereas the gradient alloy QDs rarely blink under similar imaging conditions. Despite differences in the hydrodynamic diameter between the AS-QD and GS-QD samples, both showed similar diffusional behavior. During the initial minutes (<3 min) of tracking, the MSD showed a linear relationship with time increment (see Figure 5), indicative of

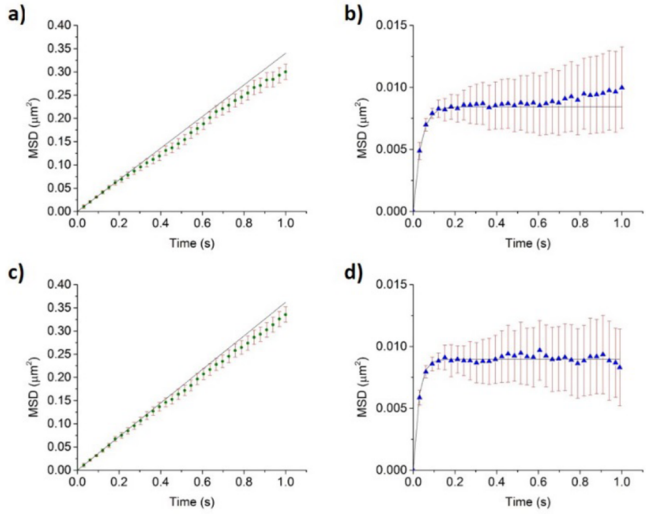

Figure 5. Plots of mean square displacement (MSD) versus time for blinking suppressed QDs in a Brownian diffusion regime where the extracted linear fit diffusion coefficient is (a) 0.085 $\mu m^2/s$, (b) blinking suppressed QDs in a confined diffusion regime where the diffusion coefficient is 0.065 $\mu m^2/s$ and the confinement length is 159 nm, (c) traditional core/shell QD in a Brownian diffusion period with diffusion coefficient of 0.091 $\mu m^2/s$, and (d) traditional QD in a confined diffusion period with a diffusion coefficient of 0.087 $\mu m^2/s$ and confinement length of 164 nm.

Brownian motion. At later time points, MSD versus time increment plots showed a plateau, indicating that the diffusion of the particles is confined to a localized region within the membrane. The switching of initial Brownian diffusion to confined diffusion behavior is commonly seen in single-particle tracking studies[19,44] and is attributed to the particles being compartmentalized within lipid rafts upon the cellular membrane.[45−47] For the Brownian regime, the free diffusion coefficients were found to be 0.085 $\mu m^2/s$ and 0.091 $\mu m^2/s$ for the AS-QDs and GS-QDs, respectively. The confinement diffusion coefficients and lengths were also similar: 0.065 $\mu m^2/s$ and 159 nm for the GS-QD and 0.087 $\mu m^2/s$ and 164 nm for the AS-QD. Similar diffusion coefficients and confinement sizes have been observed in previous membrane receptor tracking experiments using QD probes.[48] In addition, the confinement lengths are within the range of determined sizes of lipid rafts of cellular membranes (10−200 nm).[49]

Significant differences, however, were observed for the single particle trajectories in terms of frame-to-frame correlation. As shown in Figure 6, an AS-QD during an off state traveled a distance near 250 nm before reappearing. During the faster Brownian diffusion regimes in the initial stages of the imaging experiment, most AS-QDs have significant regions where there is no signal to reconstruct the trace, whereas the GS-QDs exhibited no such limitations. It was deemed that signal

dx.doi.org/10.1021/jp5064325 | J. Phys. Chem. B 2014, 118, 14140−14147

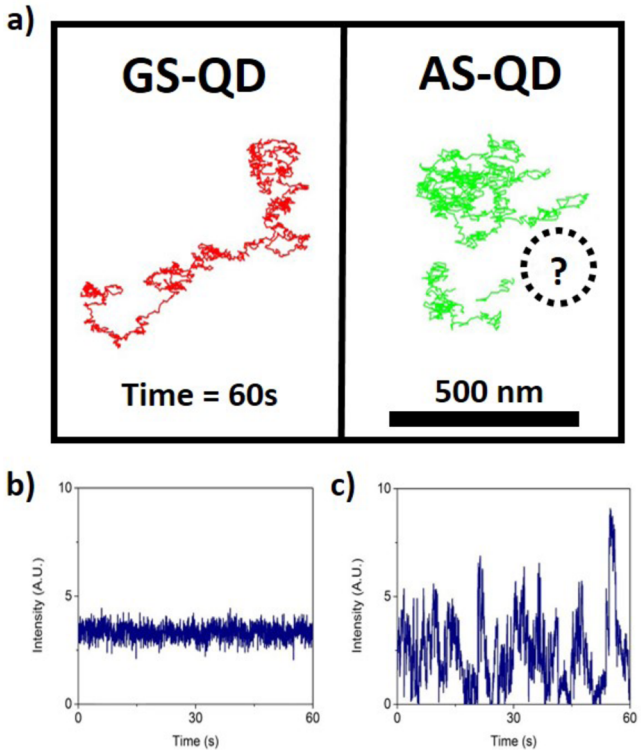

Figure 6. (a) Tracking trajectories of a gradient shell quantum dot (GS-QD) compared to a commercially available traditional abrupt shell QD (AS-QD) targeted to EGFR on live A549 cells. As can be seen in the traditional QD, prolonged "off" times gave rise to the disappearance of probe signals and a series of "blackout" frames. In contrast, blinking suppressed QDs provided continuous image frames without any gaps. Dynamic intensity traces obtained from the CCD images during a tracking study from a single GS-QD and AS-QD (b and c, respectively).

disappearances of the AS-QD were not due to movement out of the field of view as membrane undulations are smaller than the depth of field[50] and possible endosomal trafficking would not likely repeatedly return particles back to the membrane within the recorded timescales of the experiment. Additionally, if such effects were occurring, the GS-QDs should exhibit similar behaviors, which were not observed.

Dynamic intensity traces were created of single emitters using the wide-field CCD camera images, where intensity values are recorded for each frame within a 60 s stack at a 33 Hz frame rate (Figure 6). There were substantial fluctuations in the intensity profile of the AS-QD, whereas the GS-QDs have much lower variance in the intensity distribution during the 60 s interval. In addition, although the single AS-QD can yield signals almost 3 times brighter than the GS-QD in several frames, this brightness is highly unstable. Thus, an inherent advantage of greater maximum brightness of the AS-QD is rarely of significant benefit due to signal intermittency.

In conclusion, we have presented a new strategy in synthesizing blinking-suppressed, water-soluble QDs and have demonstrated their utility for live cell single-particle imaging and tracking. In particular, we have shown that linearly graded shells can be used to reduce carrier probabilities at the particle surface and also to minimize internal lattice defects at the core−shell interface. A surprising finding is that the linearly graded shells also provide an efficient insulation of the charge carriers from organic ligands, thus allowing solubilization and bioconjugation of blinking-suppressed QDs. Regarding the detailed mechanisms of QD blinking, our work has further highlighted the roles of lattice defects not only at the particle surface but also at the core−shell boundary and inside the core and shell materials.

■ ASSOCIATED CONTENT

Supporting Information

Fluorescence lifetime data; TEM, AFM, and XPS data; and quantum yields. This material is available free of charge via the Internet at http://pubs.acs.org.

■ AUTHOR INFORMATION

Corresponding Author

*E-mail: snie@emory.edu.

Notes

The authors declare no competing financial interest.

■ ACKNOWLEDGMENTS

The authors would like to thank Haijun Qian of the Clemson Electron Microscopy Facility for assistance in high-resolution TEM measurements. A.M.S. acknowledges funding from the National Institutes of Health (Grant R00CA153914). T.L. acknowledges the support from the National Science Foundation (Grant CHE-1309817). S.M.N. acknowledges support from the National Institutes of Health (Grants R01CA163256, RC2CA148265, and HHSN268201000043C).

■ REFERENCES

(1) Alivisatos, A. P.; Gu, W.; Larabell, C. Quantum dots as cellular probes. *Annu. Rev. Biomed. Eng.* **2005**, *7*, 55−76.

(2) Kairdolf, B. A.; Smith, A. M.; Stokes, T. H.; Wang, M. D.; Young, A. N.; Nie, S. Semiconductor quantum dots for bioimaging and biodiagnostic Applications. *Annu. Rev. Anal. Chem.* **2013**, *6*, 143.

(3) Kim, T.-H.; Cho, K.-S.; Lee, E. K.; Lee, S. J.; Chae, J.; Kim, J. W.; Kim, D. H.; Kwon, J.-Y.; Amaratunga, G.; Lee, S. Y. Full-colour quantum dot displays fabricated by transfer printing. *Nat. Photonics* **2011**, *5*, 176−182.

(4) Sargent, E. H. Colloidal quantum dot solar cells. *Nat. Photonics* **2012**, *6*, 133−135.

(5) Lodahl, P.; Van Driel, A. F.; Nikolaev, I. S.; Irman, A.; Overgaag, K.; Vanmaekelbergh, D.; Vos, W. L. *Nature* **2004**, *430*, 654−657.

(6) Mattoussi, H.; Kuno, M. K.; Goldman, E. R. *Optical Biosensors: Present and Future*; Liger, F. S., Taitt, C. A. R., Eds.; Elsevier: Amsterdam, 2002, 537−569.

(7) Bouzigues, C.; Levi, S.; Triller, S.; Dahan, M. *Quantum Dots Applications in Biology*; Bruchez, M., Hotz, C. Z., Eds.; Humana Press: Totowa, 2007, 81−92.

(8) Alivisatos, P. The use of nanocrystals in biological detection. *Nat. Biotechnol.* **2004**, *22*, 47−52.

(9) Medintz, I. L.; Uyeda, H. T.; Goldman, E. R.; Mattoussi, H. Quantum dot bioconjugates for imaging, labelling and sensing. *Nat. Mater.* **2005**, *4*, 435−446.

(10) Kim, S.; Lim, Y. T.; Soltesz, E. G.; De Grand, A. M.; Lee, J.; Nakayama, A.; Parker, J. A.; Mihaljevic, T.; Laurence, R. G.; Dor, D. M.; et al. Near-infrared fluorescent type II quantum dots for sentinel lymph node mapping. *Nat. Biotechnol.* **2004**, *22*, 93−97.

(11) Michalet, X.; Pinaud, F. F.; Bentolila, L. A.; Tsay, J. M.; Doose, S.; Li, J. J.; Sundaresan, G.; Wu, A. M.; Gambhir, S. S.; Weiss, S. Quantum dots for live cells, in vivo imaging, and diagnostics. *Science* **2005**, *307*, 538−544.

(12) Dabbousi, B. O.; Rodriguez-Viejo, J.; Mikulec, F. V.; Heine, J. R.; Mattoussi, H.; Ober, R.; Jensen, K. F.; Bawendi, M. G. (CdSe)ZnS core-shell quantum dots: synthesis and characterization of a size series of highly luminescent nanocrystallites. *J. Phys. Chem. B* **1997**, *101*, 9463−9475.

(13) Han, M.; Gao, X.; Su, J. Z.; Nie, S. Quantum-dot-tagged microbeads for multiplexed optical coding of biomolecules. *Nat. Biotechnol.* **2001**, *19*, 631−635.
(14) Smith, A. M.; Nie, S. Bright and compact alloyed quantum dots with broadly tunable near-infrared absorption and fluorescence spectra through mercury cation exchange. *J. Am. Chem. Soc.* **2011**, *133*, 24−26.
(15) Yildiz, A.; Forkey, J. N.; McKinney, S. A.; Ha, T.; Goldman, Y. E.; Selvin, P. R. Myosin V walks hand-over-hand: single fluorophore imaging with 1.5-nm localization. *Science* **2003**, *300*, 2061−2065.
(16) Clausen, P. M.; Lagerholm, C. B. The probe rules in single particle tracking. *Curr. Protein Pept. Sci.* **2011**, *12*, 699−713.
(17) Wieser, S.; Schütz, G. J. Tracking single molecules in the live cell plasma membrane-do's and don't's. *Methods* **2008**, *46*, 131−140.
(18) Calamai, M.; Specht, C. G.; Heller, J.; Alcor, D.; Machado, P.; Vannier, C.; Triller, A. Gephyrin oligomerization controls GlyR mobility and synaptic clustering. *J. Neurosci.* **2009**, *29*, 7639−7648.
(19) Chang, Y. P.; Pinaud, F.; Antelman, J.; Weiss, S. Tracking bio-molecules in live cells using quantum dots. *J. Biophotonics* **2008**, *1*, 287−298.
(20) Groc, L.; Lafourcade, M.; Heine, M.; Renner, M.; Racine, V.; Sibarita, J.-B.; Lounis, B.; Choquet, D.; Cognet, L. Surface trafficking of neurotransmitter receptor: Comparison between single-molecule/quantum dot strategies. *J. Neurosci.* **2007**, *27*, 12433−12437.
(21) Jaqaman, K.; Loerke, D.; Mettlen, M.; Kuwata, H.; Grinstein, S.; Schmid, S. L.; Danuser, G. Robust single-particle tracking in live-cell time-lapse sequences. *Nat. Methods* **2008**, *5*, 695−702.
(22) Sergé, A.; Bertaux, N.; Rigneault, H.; Marguet, D. Dynamic multiple-target tracing to probe spatiotemporal cartography of cell membranes. *Nat. Methods* **2008**, *5*, 687−694.
(23) Schwille, P.; Korlach, J.; Webb, W. W. Fluorescence correlation spectroscopy with single-molecule sensitivity on cell and model membranes. *Cytometry* **1999**, *36*, 176−182.
(24) Hohng, S.; Ha, T. Near-complete suppression of quantum dot blinking in ambient conditions. *J. Am. Chem. Soc.* **2004**, *126*, 1324−1325.
(25) Chen, Y.; Vela, J.; Htoon, H.; Casson, J. L.; Werder, D. J.; Bussian, D. A.; Klimov, V. I.; Hollingsworth, J. A. "Giant" multishell CdSe nanocrystal quantum dots with suppressed blinking. *J. Am. Chem. Soc.* **2008**, *130*, 5026−5027.
(26) Mahler, B.; Spinicelli, P.; Buil, S.; Quelin, X.; Hermier, J.-P.; Dubertret, B. Towards non-blinking colloidal quantum dots. *Nat. Mater.* **2008**, *7*, 659−664.
(27) Cragg, G. E.; Efros, A. L. Suppression of Auger processes in confined structures. *Nano Lett.* **2010**, *10*, 313−317.
(28) Wang, X.; Ren, X.; Kahen, K.; Hahn, M. A.; Rajeswaran, M.; Maccagnano-Zacher, S.; Silcox, J.; Cragg, G. E.; Efros, A. L.; Krauss, T. D. Non-blinking semiconductor nanocrystals. *Nature* **2009**, *459*, 686−689.
(29) Nakagawa, Y.; Nakajima, K.; Tayama, S.; Moldéus, P. Metabolism and cytotoxicity of propyl gallate in isolated rat hepatocytes: Effects of a thiol reductant and an esterase inhibitor. *Mol. Pharmacol.* **1995**, *47*, 1021−1027.
(30) Gregory, L.; Davis, K. G.; Sheth, B.; Boyd, J.; Jefferis, R.; Nave, C.; Burton, D. R. The solution conformations of the subclasses of human IgG deduced from sedimentation and small angle X-ray scattering studies. *Mol. Immunol.* **1987**, *24*, 821−829.
(31) Qin, H.; Niu, Y.; Meng, R.; Lin, X.; Lai, R.; Fang, W.; Peng, X. Single-dot spectroscopy of zinc-blende CdSe/CdS core/shell nanocrystals: Nonblinking and correlation with ensemble measurements. *J. Am. Chem. Soc.* **2014**, *136*, 179−187.
(32) Chen, O.; Zhao, J.; Chauhan, V. P.; Cui, J.; Wong, C.; Harris, D. K.; Wei, H.; Han, H.-S.; Fukumura, D.; Jain, R. K.; et al. Compact high-quality CdSe−CdS core−shell nanocrystals with narrow emission linewidths and suppressed blinking. *Nat. Mater.* **2013**, *12*, 445−451.
(33) Mei, B. C.; Susumu, K.; Medintz, I. L.; Delehanty, J. B.; Mattoussi, H. Modular poly (ethylene glycol) ligands for biocompatible semiconductor and gold nanocrystals with extended pH and ionic stability. *Proc. SPIE* **2008**, *18*, 4949−4958.
(34) Smith, A. M.; Nie, S. Bioconjugated quantum dots for in vivo molecular and cellular imaging. *J. Am. Chem. Soc.* **2008**, *130*, 11278−11279.
(35) Kang, E.; Ogura, A.; Kataoka, K.; Nagasaki, Y. Preparation of water-soluble PEGylated semiconductor nanocrystals. *Chem. Lett.* **2004**, *33*, 840−841.
(36) Riddoch, F. A.; Jaros, M. Local Auger effects at point defects in silicon. *J. Phys. Chem. C* **1980**, *13*, 6181.
(37) Molina, S. I.; Pacheco, F. J.; Araujo, D.; Garcia, R.; Sacedon, A.; Calleja, E.; Yang, Z.; Kidd, P. Design of InGaAs linear graded buffer structures. *Appl. Phys. Lett.* **1994**, *65*, 2460−2462.
(38) Tersoff, J. Dislocations and strain relief in compositionally graded layers. *Appl. Phys. Lett.* **1993**, *62*, 693−695.
(39) Kuno, M.; Fromm, D.; Hamann, H.; Gallagher, A.; Nesbitt, D. Nonexponential "blinking" kinetics of single CdSe quantum dots: A universal power law behavior. *J. Chem. Phys.* **2000**, *112*, 3117−3120.
(40) Chung, I.; Bawendi, M. G. Relationship between single quantum-dot intermittency and fluorescence intensity decays from collections of dots. *Phys. Rev. B* **2004**, *70*, 165304.
(41) Jin, S.; Song, N.; Lian, T. Suppressed blinking dynamics of single QDs on ITO. *ACS Nano* **2010**, *4*, 1545−1552.
(42) Fisher, B. R.; Eisler, H.-J.; Stott, N. E.; Bawendi, M. G. Type-II quantum dots: CdTe/CdSe (core/shell) and CdSe/ZnTe (core/shell) heterostructures. *J. Phys. Chem. B* **2004**, *108*, 143−148.
(43) Xie, R.; Kolb, U.; Li, J.; Basché, T.; Mews, A. Synthesis and characterization of highly luminescent CdSe−Core CdS/$Zn_{0.5}Cd_{0.5}S$/ZnS multishell nanocrystals. *J. Am. Chem. Soc.* **2005**, *127*, 7480−7488.
(44) Bannai, H.; Lévi, S.; Schweizer, C.; Dahan, M.; Triller, A. Imaging the lateral diffusion of membrane molecules with quantum dots. *Nat. Protoc.* **2007**, *1*, 2628−2634.
(45) Dietrich, C.; Yang, B.; Fujiwara, T.; Kusumi, A.; Jacobson, K. Relationship of lipid rafts to transient confinement zones detected by single particle tracking. *Biophys. J.* **2002**, *82*, 274−284.
(46) Triantafilou, M.; Morath, S.; Mackie, A.; Hartung, T.; Triantafilou, K. Lateral diffusion of Toll-like receptors reveals that they are transiently confined within lipid rafts on the plasma membrane. *J. Cell Sci.* **2004**, *117*, 4007−4014.
(47) Fujiwara, T.; Ritchie, K.; Murakoshi, H.; Jacobson, K.; Kusumi, A. Phospholipids undergo hop diffusion in compartmentalized cell membrane. *J. Cell Biol.* **2002**, *157*, 1071−1082.
(48) Clausen, M. P.; Lagerholm, B. C. Visualization of Plasma Membrane Compartmentalization by High-Speed Quantum Dot Tracking. *Nano Lett.* **2013**, *13*, 2332−2337.
(49) Pike, L. J. The challenge of lipid rafts. *J. Lipid. Res.* **2009**, *50*, S323−S328.
(50) Domke, J.; Parak, W. J.; George, M.; Gaub, H. E.; Radmacher, M. Mapping the mechanical pulse of single cardiomyocytes with the atomic force microscope. *Eur. Biophys. J.* **1999**, *28*, 179−186.